# Velocity Vector Analysis of a Juncture Flow Using a Three-Component Laser Velocimeter

**James F. Meyers**
**NASA Langley Research Center**
**Hampton, Virginia 23665**

**and**

**Timothy E. Hepner**
**U. S. Army R&T Labs (AVRADCOM)**
**Hampton, Virginia 23665**

**Second International Symposium on**
**Applications of Laser Anemometry**
**to Fluid Mechanics**
**July 2-4, 1984**
**Lisbon, Portugal**

# Velocity Vector Analysis of a Junction Flow Using A Three Component Laser Velocimeter

James F. Meyers
NASA Langley Research Center
Hampton, VA 23665, USA

and

Timothy E. Hepner
U.S. Army R&T Labs (AVRADCOM)
Hampton, VA 23665, USA

## Abstract

A specialized single-axis, five-beam three-component laser velocimeter was constructed and used to study the flow field in a juncture. The juncture was defined by a blunt leading, edged vertical splitter plate and a sharp leading edged horizontal plate. The investigations were conducted in the Low Turbulence Pressure Tunnel at a Mach number of 0.1 and a Reynolds number of $2.2 \times 10^6$ per meter over the model. The three-component velocity flow field in the juncture was measured, Reynolds stresses calculated and the velocity vector analysis performed.

## Introduction

There are several basic flow field situations in the field of fluid mechanics which should be well understood since they occur so often, but instead very little is known about them. One such situation is the flow field in the immediate vicinity of a juncture. One reason for this paucity of knowledge of the juncture flow is due to the difficulty in using classic probe techniques to measure complex three-dimensional flow fields without influencing the flow under investigation. An earlier attempt to study this flow using hot wire anemometry, reference 1, has indicated the presence of a vortex near the juncture. Although this study has added to the understanding of the flow field, the degree of influence due to the presence of the probe on the flow is unknown.

A solution to the probe interference problem is to investigate the flow field with a nonintrusive flow diagnostic technique such as laser velocimetry. Laser velocimetry offers the necessary measurement capabilities to define the flow in a juncture, but the use of the technique

places requirements on the tunnel and the model especially when three-component measurements are needed. The two major problem areas in the present study were optical access (limited by the model and the tunnel structure to a single window), and wall flare which limits the approach to the juncture. Of the three-component configurations presented in the literature, references 2-5, the single-axis, five-beam technique presented in reference 5 needed only a single window and could be modified to collect the scattered light off-axis minimizing the effects of wall flare. The optics system produced a sample volume 80 micrometers in diameter by 120 micrometers in length and yielded 0.4 volt peak-to-peak signals from 0.5 micron polystyrene particles during laboratory tests. The small sample volume and off-axis collection of the scattered light allowed velocity measurements to be made to within 1.0 mm of the horizontal surface and to within 3.5 mm of the vertical surface of the juncture. The requirement of coincidence between all three velocity components was imposed upon the data acquisition system to permit velocity vector analysis and measurement of Reynolds stress. The resulting measurements were processed in the manner described in reference 6 to insure the independence of the individual realizations which comprise a measurement data ensemble removing any effects of velocity bias.

## Wind Tunnel and Model Configuration

The Low Turbulence Pressure Tunnel is a closed circuit, single-return, pressure tunnel which can be operated at pressures from 0.1 atmosphere to 10.0 atmospheres. The total temperature may be varied from ambient to 50 degrees Celsius and the free stream Mach number may be varied from 0.02 to 0.53. The tunnel has less than 0.1 percent free stream turbulence (measured with hot wire anemometry). The test section is 0.91 m wide by 2.29 m high with a model support system consisting of rotating plates on either side of the tunnel to support two dimensional airfoil research. In the present study, one of the rotating plates was replaced with a 0.75 m diameter window to allow optical access for the laser velocimeter.

The model consisted of a vertical splitter plate placed 0.15 m off of the far wall (opposite of the window location) and hard mounted to the floor and ceiling. The splitter plate had a flat surface with a blunt leading edge and a chord length of 1.219 m. A horizontal plate was hard mounted to the splitter plate and a vertical support structure located 0.01 m from the window. The leading edge of the horizontal plate was located 0.406 m downstream from the leading edge of the splitter plate. The horizontal plate had a sharp leading edge and was flat on one side and curved (0.838 m radius of curvature) on the other. The horizontal plate

had a chord length of 0.457 m and a span of 0.15 m. Deflection spoilers were placed on the horizontal plate and splitter plate trailing edges to maintain stable flow over the model. The flow field under investigation was located in the upper juncture defined by the splitter and the horizontal plates. The juncture shapes could be modified by using various fillets. The present test used a square corner fillet and a curved (0.0254 cm radius of curvature) fillet. A photograph of the model is shown in Figure 1.

## Laser Velocimeter

The three dimensional nature of the flow field in a juncture required the design of a three-component laser velocimeter. The design of the system was complicated by the limited optical access, a single 0.75 m diameter window, that ruled out the forward scatter optical configurations and the orthogonal approach, reference 2, to measure the cross flow component. The location of the window in the model support structure added the complication of being surrounded by a drum 0.976 m in diameter by 0.711 m in depth. The limited area within the drum precluded the use of the off-axis approach, reference 3, to measure the cross flow component. The direct-backscatter, reference-beam technique, reference 4, to measure the cross flow component was also rejected since background reflections from the vertical splitter plate would overwhelm the scattered light from the particles. The single-axis, five-beam configuration, reference 5, utilizes a modified standard two-color fringe-type system with a fifth beam placed along the optical axis which creates two additional fringe patterns to measure the cross flow component. This technique was chosen for the present study because the optical system could be constructed small enough to operate within the confines of the drum and off-axis collection of the scattered light could be used to reduce the effect of background reflections from the splitter plate.

### Optical System Operation

The single-axis, five-beam optical configuration, uses the standard two-color, two component beam pattern with the two green beams (514.5 nm) arranged in the horizontal plane and the two blue beams (488.0 nm) arranged in the vertical plane forming a diamond pattern to measure the $U$ or streamwise component (green beams) and the $V$ or vertical component (blue beams). A third green beam is placed along the optical axis bisecting the angle between the original two green beams. The addition of this beam will create two additional fringe patterns within the sample volume. These additional fringe patterns are inclined

symmetrically about the optical axis yielding equal contributions of the $U$ component and equal but opposite contributions of the $W$ or cross flow component. The $W$ velocity component can then be obtained from the difference of the two signal frequencies.

The three signals obtained from the three green fringe patterns can be separated by frequency if Bragg cells are included in the two outside beams. A 60 MHz Bragg cell was placed in the left green beam to shift the optical frequency above the base frequency and a 40 MHz Bragg cell was placed in the right green beam to shift the optical frequency below the base frequency. This results in a 100 MHz difference between the outside two beams, a 60 MHz difference between the left pair, and a 40 MHz difference between the right pair. The three signal frequencies with their respective frequency biases can be isolated by electronic filters provided the component velocities are sufficiently small. The filter network, shown schematically in Figure 2, isolates the $U$-component signal frequency and the two signal frequencies from the inclined fringe patterns which are then input to an electronic double balanced mixer. The lower frequency signal from the mixer in the frequency difference between the two input signals and is the $W$-component signal frequency biased by 20 MHz.

The conversion of the measured signal frequency values for the $U$ and $V$ components is via the standard conversion equation:

$$U,\ V\ = \frac{\lambda\,(f - f_B\,)}{2\sin\ \frac{\theta}{2}} \qquad (1)$$

where $\lambda$ is 514.5 nm for the $U$ component and 488.0 nm for the $V$ component and the subtracted Bragg bias frequency, $f_B$, is 40 MHz for the $U$ component and 10 Hz for the $V$ component. The original Bragg bias frequencies were subsequently reduced via down mixing with electronic mixers and reference signals obtained from derivatives of the original Bragg cell drive signals. The conversion of the signal frequency value for the $W$ component requires modification of equation (1) to include contributions from both fringe patterns and orientation of the patterns with respect to the $W$ axis which is $\theta/4$. The equation for $W$ is then expressed as:

$$W\ = \frac{\lambda\,(f - f_B\,)}{4\sin^{\,2}\ \frac{\theta}{4}} \qquad (2)$$

where $\lambda$ is 514.5 nm and the subtracted Bragg bias frequency, $f_B$, which has been down mixed to 5 MHz.

## Optical System Design

The design of the optical system must include the limitations due to the tunnel and the model configurations and measurement requirements. These requirements include: a sample volume length of less than 0.5 mm to minimize velocity gradient averaging within the boundary layer, full directionality capabilities in all three components, the ability to measure the flow field to within 5.0 mm of the vertical splitter plate and to within 2.0 mm of the horizontal plate, and the ability to obtain usable signals from 0.5 micron diameter particles to guarantee particle tracking fidelity.

The relationship between the cross beam angle and output beam diameter is determined by the requirement that the sample volume length must be less than 0.5 mm. Assuming diffraction limited optics, equations (3) and (4) define the beam waist diameter (half power points), $D$, and the sample volume length, $L$, respectively:

$$D = \frac{4 \lambda F}{\pi d} \tag{3}$$

$$L = \frac{\sqrt{2}\ D}{\sin \theta} \tag{4}$$

Using 514.5 nm for the laser wavelength, $\lambda$, 1.0 m for the system focal length, $F$, and the required 0.5 mm sample volume length, $L$, the cross beam angle, $\theta$, in related to the output beam diameter, $d$, by:

$$\theta = \sin^{-1} \left( \frac{0.00185}{d} \right) \tag{5}$$

The determination of the cross beam angle and the output beam diameter may be made by specifying the effective Bragg bias frequency and the maximum expected velocity magnitude. The effective Bragg bias frequency in the $W$ component was chosen to be 5 MHz to minimize quantizing error in the high-speed burst counter. The maximum expected velocity above the curved surface is 45 m/sec. The minimum sample volume diameter can then be determined since the high-speed burst counter requires ten cycles within the signal burst, a particle must remain within the sample volume for two microseconds to obtain a measurement of the $W$ component. Therefore the sample volume must

be 90 micrometers or larger for a particle velocity of 45 m/sec. Using equations (3), (4), and (5), the minimum cross beam angle is found to be 15 degrees with an output beam diameter of 7.16 mm.

Using 15 degrees as the design cross beam angle, the beam separation distance at the final lens becomes 0.263 m. This would make the desired lens diameter 0.33 m to keep the beams away from aberrations normally present at the edge of a lens. Unfortunately, an f/3 lens of this diameter was cost prohibitive. An alternate approach was to use a system of mirrors to separate and steer the beams to obtain the required cross beam angle of 15 degrees and five telescopes to obtain the proper output beam diameter.

The diameter of the scattered light collecting lens was determined using the laser velocimeter simulation program, reference 7. The input to the program specified the characteristics of the transmission optics, a collecting lens location between two of the outside telescopes, and a 0.5 micron polystyrene particle traveling at a velocity of 45 m/sec. Requiring a peak-to-peak signal voltage of 0.5 volts resulted in the program specifying a collecting lens diameter of 0.152 m.

The optical system was then constructed and tested in the laboratory using a small jet seeded with 0.5 micron polystyrene particles and a polished aluminum angle painted flat black to simulate the juncture. Peak-to-peak signals of 0.4 volts were obtained to within 1.0 mm of the horizontal surface and to within 3.5 mm of the vertical surface where flare reduced the signal-to-noise ratio below usable limits. The system was then mounted on a three degree of freedom traversing mechanism in the final configuration, Figure 3, and tested again with the same results.

## Error Analysis

An error analysis was performed on the system using the procedures outlined in references 8 and 9. The analysis indicated that the only error in the measurement of the mean was due to the uncertainty in the measurement of the cross beam angle: 0.2 percent in $U$ and $V$ and 0.4 percent in $W$. The remaining errors are correctable (velocity bias and clock synchronization) or are not applicable (Bragg bias, nonparallel fringes, time jitter in the counter, and particle lag). The two errors affecting the measurement of the turbulence intensity were quantizing error in the counter (correctable), and error due to velocity gradients within the sample volume (worst case of 1.2 percent based on the mean velocity measurements through the boundary layer). The statistical uncertainties were determined for each ensemble during data

processing and were based on the number of independent measurements of the flow. The average statistical uncertainty in the mean was about 1 percent and the average uncertainty in the turbulence intensity was about 1 percent.

### Data Acquisition System

The signals from the optics system were processed using high-speed burst counters with a 500 MHz reference clock frequency ($U$ and $V$ components) and a 1 GHz reference clock frequency ($W$ component). The digital output from each counter was input into a parallel data acquisition unit (LVABI, reference 10) for intermediate data storage. The LVABI also established the coincidence condition between the components for later velocity vector analysis and measured the time between successive coincident measurements for later determination of the flow correlation time. The coincidence time window was chosen to be 5 microseconds to account for the expected minimum particle transit time through the sample volume and the difference between the data validation pulses from the high-speed burst counters. Once the measurement ensemble was obtained in the LVABI, the data was transferred to a minicomputer for real time processing of the component statistics and final data storage.

### Particle Generator

The seeding particles were generated in the tunnel using a mechanical atomizer with tridecane as the particle material. The generator was attached to a traversing mechanism which was mounted to the tunnel support structure just upstream of the tunnel screens in the settling chamber. Tridecane was chosen as the particle material because of its relatively high vapor pressure and purity. These characteristics kept the particle size small and did not allow deposits to form on the fine mesh tunnel screens. A comparison of signal voltages from the 0.5 micron polystyrene particles and the tridecane particles indicated that the tridecane particles were approximately 0.4 microns in diameter.

## The Experiment

The optical system and traversing mechanism were installed in the plenum chamber, Figure 4, and the data acquisition system placed in the control room adjacent to the tunnel. The tunnel was set to a free stream Mach number of 0.1 at atmospheric pressure and a total temperature of

27 degrees Celsius yielding a Reynolds number of $2.2 \times 10^6$ per meter over the model. The measurements were made over a 3.0 cm by 3.0 cm grid in the $Y$ (vertical direction) and $Z$ (cross flow direction) plane in the juncture. The grid encompassed 210 measurement locations taken every 1 mm within 1 cm of the horizontal plate surface and 2 mm above along scan lines every 2.5 mm parallel to the vertical splitter plate. The flow field was measured at the 50-, 75-, and 95-percent chord positions along the horizontal plate. The flat and curved surfaces with the square corner and the curved (0.0254 m radius of curvature) juncture were studied. The repeatability of the measurements was tested by returning to the $Y$ = 3.0 cm, $Z$ = 3.0 cm position following each vertical scan and comparing the measured results. The mean velocities in all three components, $U$, $V$, and $W$, (32.9 m/sec, 0.858 m/sec and -0.206 m/sec, respectively) typically repeated to within 0.3 m/sec and the turbulence intensities (0.038, 0.00587, and 0.097, respectively) repeated to within 0.005. The measurements at the $Y$ = 3.0 cm, $Z$ = 3.0 cm location were also used to correct minor changes in the mean velocity in the $W$ component as the optical alignment drifted due to tunnel vibration. (A difference in cross beam angle between the three output beams of 0.0003 degree results in an artificial velocity in the $W$ component of 1.5 m/sec).

## Data Analysis

The laser velocimeter measures velocity events that are approximately Poisson distributed in time at a location in the flow yielding a sample of the velocity flow field taken over a finite period of time. As with any flow diagnostic measurement, it is assumed that the statistical analysis of the measured ensemble is a good representation of the stationary flow field characteristics at that location. This assumption is valid if 1) the flow field is indeed stationary, and 2) the particle arrivals are truly Poisson distributed in time yielding independent samples of the flow field. The independence of the samples has been questioned by several researchers, references 11-13, in that they hypothesize that there is a dependence of the particle arrival rate on velocity.

### Velocity Bias

The hypothesis, referred to as velocity bias, states that if the particles are uniformly distributed in space, the higher velocities at a location will pass more fluid and thus more particles through the sample volume than lower velocities per unit time. This results in a bias toward the higher velocity when standard statistical analyses are performed on the data ensemble. Recent theoretical efforts, references 14 and 15, have

questioned this hypothesis based on whether or not more than one velocity measurement was obtained within the flow correlation time. If the data rate is high more than one measurement per correlation time the adjacent data points are related to each other due to the flow turbulence regardless of any velocity bias. Since this appears to be the case in references 12 and 13, their experimental conclusions about velocity bias are questionable. The experimental study conducted in reference 2, which compared laser velocimeter measurements with hot wire measurements obtained at the same time in approximately the same location (the hot wire was located 2 mm downstream of the laser velocimeter sample volume), showed that the difference between the two measurements was larger when the velocity bias correction from reference 11 was applied. This result prompted testing of the basic hypothesis by calculating the correlation coefficient between the measured velocity and data rate. Using the measured flow correlation time obtained from the hot wire, the measured laser velocimeter time record was segmented in units of correlation time. The instantaneous velocity, $U_j$, was determined by averaging the velocity measurements within each correlation time segment and the instantaneous data rate, $r_j$, was determined by dividing the number of measurements within each time segment by the correlation time. These values were then entered into equation (6) and the correlation coefficients, C, determined for all measurement locations in the flow.

$$C = \frac{\left(U_j - \overline{U}\right)\left(r_j - \bar{r}\right)}{\sigma_U \, \sigma_r} \tag{6}$$

The correlation coefficient was found to be randomly distributed with small values, less than 0.1, within the jet and rose to 0.4 at the edge of the flow where clean entrained air of low velocity was present. It was therefore concluded that in general classical velocity bias was not present and that the dependence of data rate upon velocity was small. Although the dependence was small, for maximum measurement accuracy a technique was needed to completely remove the dependence leaving an ensemble of independent velocity measurements.

Such a technique has been developed in reference 6 which, when applied to the data from reference 2, yielded better measurement comparisons, (less than 1 percent difference) between the laser velocimeter data and the hot wire data than the uncollected data (5 percent difference) or the velocity bias corrected (reference 11) data (10 percent difference). These favorable comparisons were maintained for correlation coefficients of 0 to correlation coefficients of 0.4. This technique removes any dependence of one velocity measurement upon another regardless of the source of the dependency by determining the arrival

rate transfer function and limiting the data to one velocity measurement per correlation time.

## Data Processing

Each of the velocity ensembles was processed in accordance with the technique outlined in reference 6 to remove any dependence of one velocity measurement upon another. The means, statistical uncertainties in the means (based on the number of correlation times, i.e., independent measurements), standard deviations (where applicable, turbulence intensity values, i.e., standard deviation divided by the local mean $U$ component of velocity), statistical uncertainties in the standard deviations, skew, excess, correlation times, and the number of correlation times in the measurement ensemble were calculated. Corrections for high-speed burst counter clock synchronization and quantizing error were made to the $U$ component of velocity and the velocity magnitude. The correlation coefficient between the $U$-component velocity and data rate and Reynolds stress between the component pairs (boundary layer coordinates) were calculated using standard statistics.

## Results

Typical results are presented in a contour mapping format to allow a global view of the flow field. The results presented in Figures 5-11 were obtained at the 95 percent chord location of the flat horizontal plate with a square corner juncture. The $U$ component of velocity, shown in Figure 5, indicates a 1.0 cm thick boundary layer above the horizontal plate and a 1.5 cm thick boundary layer next to the vertical splitter plate. The $U$-component turbulence intensity (based on local mean velocity in the $U$ component), Figure 6, increases as expected within the boundary layers. The mean velocities in the $V$ component, Figure 7, and in the $W$ component, Figure 8, are small with no apparent flow structure. By calculating the velocity vector magnitude in the $Y$-$Z$ plane ($V$ and $W$ velocity components) and determining the flow angle gamma ($\gamma$ = arc tan ($W/V$)) and presenting the results in a vector plot, Figure 9, a structure appears to be present with the flow going into the juncture from above and leaving along the horizontal plate. The Reynolds stress results shown in Figure 10 appear to follow the classic form along each wall, however the upswing to a value of zero is not seen because wall flare prevented measurements within the final 28 percent of the boundary layer. The map of the correlation coefficients between the $U$ component of velocity and data rate, Figure 11, shows a random correlation with magnitudes below 0.4 with as much negative

correlation occurring as the expected positive correlation due to velocity bias.

## Concluding Remarks

The flow field in a juncture has been studied using a specialized single-axis, three-component laser velocimeter. The system produced a sample volume 60 micrometers in diameter by 120 micrometers in length and used off-axis collection of the scattered light to minimize background light from wall flare. This allowed velocity measurements to be made to within 1.0 mm off of the horizontal plate and to within 3.5 mm of the vertical splitter plate. Full coincidence between the three components was imposed to allow velocity vector analysis of the flow, rotation of the coordinate system to align with the boundary layer coordinate system, and calculation of the Reynolds stresses. The data was processed in a manner to obtain statistically independent measurement samples which eliminated velocity bias. An error analysis verified by repeatability tests in the wind tunnel indicated that the $U$, $V$, and $W$ velocity component measurements had less than 1 percent scatter (normalized by free stream velocity). Typical three dimensional profiles and a vector plot of the data obtained from the flow field in the juncture for a flat plate with a square corner have been presented.

## Acknowledgment

The authors wish to acknowledge the contributions of Dr. James Scheiman, who, as principal investigator for the specific experiments described in this paper, was responsible for the tunnel operations, preparation and operation of the seeding system and the experimental model. The authors also wish to thank the technicians of the Low Turbulence Pressure Tunnel whose efforts contributed significantly to the success of the overall test program.

## References

1. McMahon, H.; Hubbartt, J.; and Kubendran, L. R.: *Mean Velocities and Reynolds Stresses Upstream of a Simulated Wing-Fuselage Juncture*, NASA CR-3695, June 1983.

2. Meyers, J. F.; and Wilkinson, S. P.: *A Comparison of Turbulence Intensity Measurements Using a Laser Velocimeter and a Hot Wire in a Low Speed Jet Flow*, International Symposium on

Applications of Laser-Doppler Anemometry to Fluid Mechanics, Lisbon, Portugal, July 5-7, 1982.

3. Yanta, W. J.; and Ausherman, D. W.: *Application of the Laser Doppler Velocimeter in Aerodynamic Flows*, Proceedings of a Workshop on Flow Visualization and Laser Velocimetry for Wind Tunnels, NASA CP-2243, March 25-26, 1982.

4. Orloff, K. L.; and Logan, S. E.: *Confocal Backscatter Laser Velocimeter with On-Axis Sensitivity*, Applied Optics, Vol. 12, no. 10, pp. 2477-2481, October 1973.

5. Schock, H. J.; Began, C. A.; Rice, W. J.; and Chlebeck, R. A.: *Multicomponent Velocity Measurement in a Piston-Cylinder Configuration Using Laser Velocimetry*, TSI-Quarterly, Vol. 9, Issue 4, Oct-Dec 1983.

6. Edwards, R. V.; and Meyers, J. F.: *An Overview of Particle Sampling Bias*, Second International Symposium on Applications of Laser Anemometry to Fluid Mechanics, Lisbon, Portugal, July 2-4, 1984.

7. Meyers, J. F.: *Investigation and Calculations of Basic Parameters for the Application of the Laser Velocimeter*, NASA TND-6125, April 1971.

8. Meyers, J. F.: *Applications of Laser Velocimetry to Large Scale and Specialized Aerodynamic Tests*, TSI-Quarterly, Vol. V, Issue 4, Nov-Dec 1979.

9. Gartrell, L. R.; Gooderum, P. B.; Hunter, W. W., Jr.; and Meyers, J. F.: *Laser Velocimetry Technique Applied to the Langley 0.3-meter Transonic Cryogenic Tunnel*, NASA TM-81913, April 1981.

10. Meyers, J. F.; and Clemmons, J. I., Jr.: *Processing Laser Velocimeter High-Speed Burst Counter Data*, Third International Workshop on Laser Velocimetry, Purdue University, July 1978.

11. Tiedermann, W. G.; McLaughlin, D. K.; and Reischman, M. M.: *Individual Realization Laser Doppler Technique Applied to Turbulent Channel Flow*, Proceedings of Symposium on Turbulence in Liquids, Rolla, Missouri, 1973.

12. Roesler, T.; Stevenson, W. H.; and Thompson, H. D.: *Investigation of Bias Errors in Laser Doppler Velocimeter Measurements*, AFWAL TR-80-2108, December 1980.

13. Johnson, D. A.; Modarress, D.; and Owen, F. K.: *An Experimental Verification of Laser-Velocimeter Sampling Bias Correction*, Proceedings of the Symposium on Engineering Applications of Laser Velocimetry, ASME Winter Annual Meeting, Phoenix Arizona, November 1982.

14. Erdmann, J. C.; and Tropea, C.: *Statistical Bias of the Velocity Distribution Function in Laser Anemometry*, International Symposium on Applications of Laser-Doppler Anemometry to Fluid Mechanics, Lisbon, Portugal, July 5-7, 1982.

15. Edwards, R. V.; and Jensen, A. S.: *Output Statistics of Laser Anemometers in Sparsely Seeded Flows,* International Symposium on Applications of Laser-Doppler Anemometry to Fluid Mechanics, Lisbon, Portugal, July 5-7, 1982.

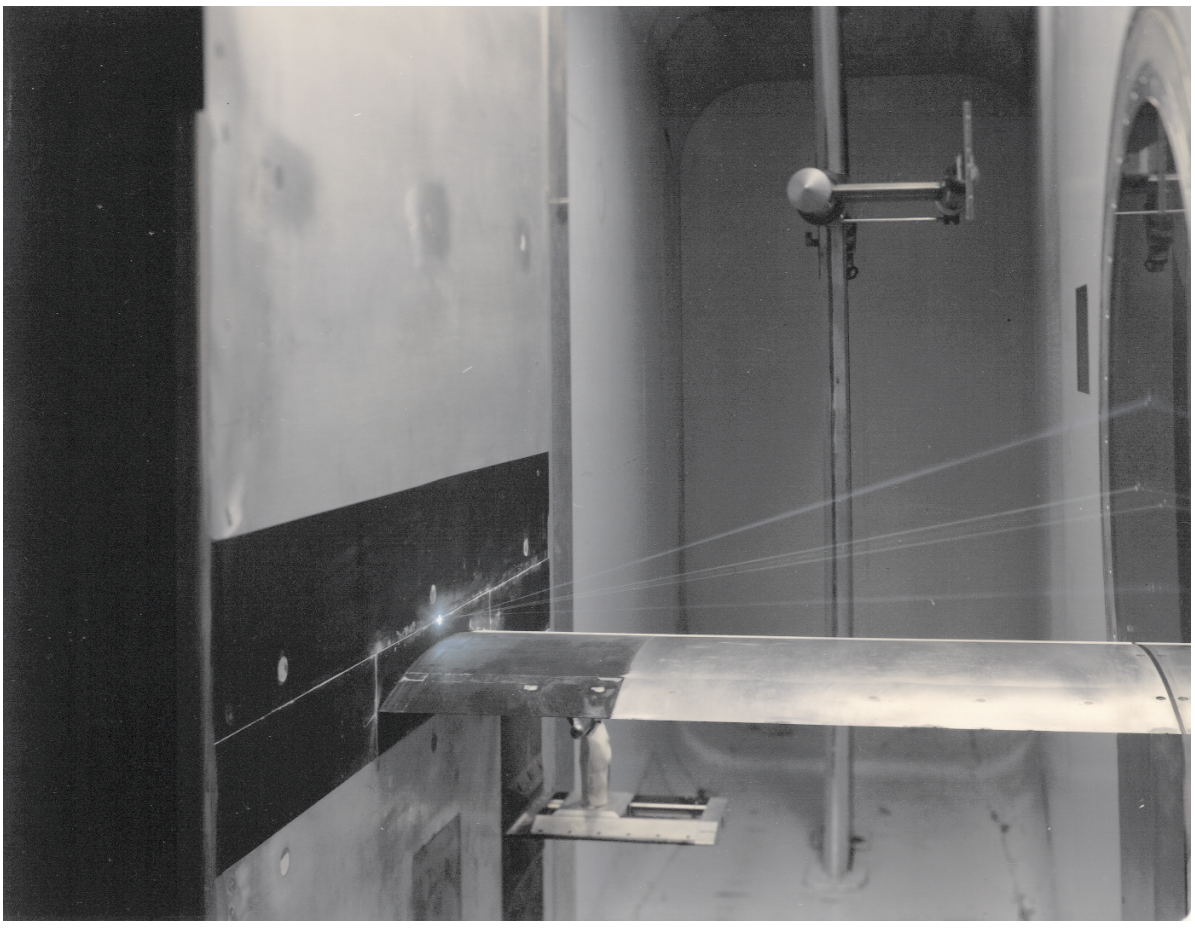

Figure 1.- Juncture Flow Model

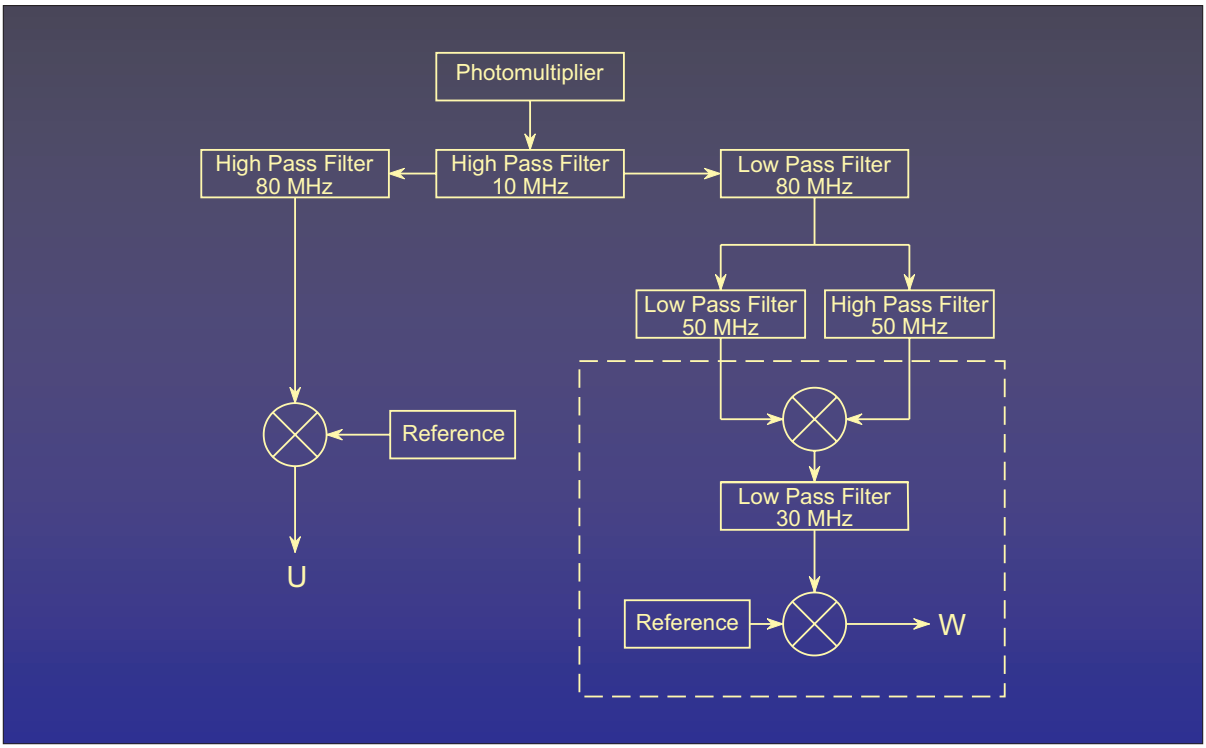


Figure 2.- Signal Separation Electronics for the $U$ and $W$ Components.

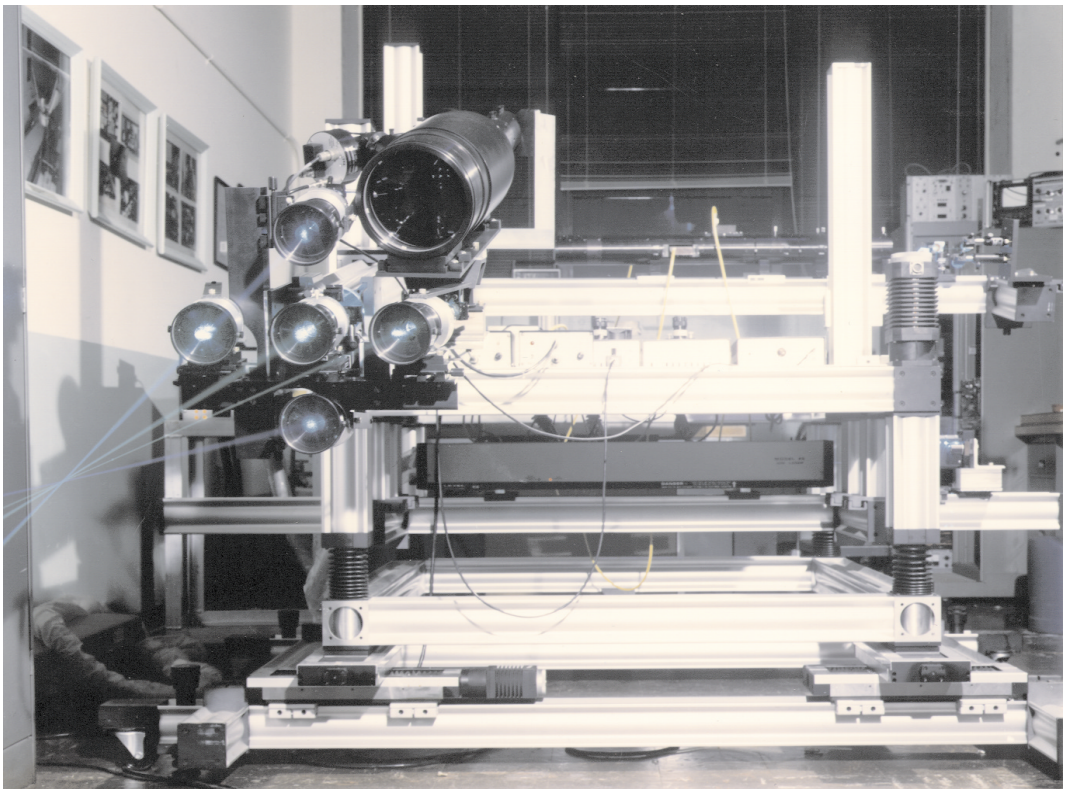

Figure 3.- Single-Axis, Five-Beam, Three-Component Laser Velocimeter.

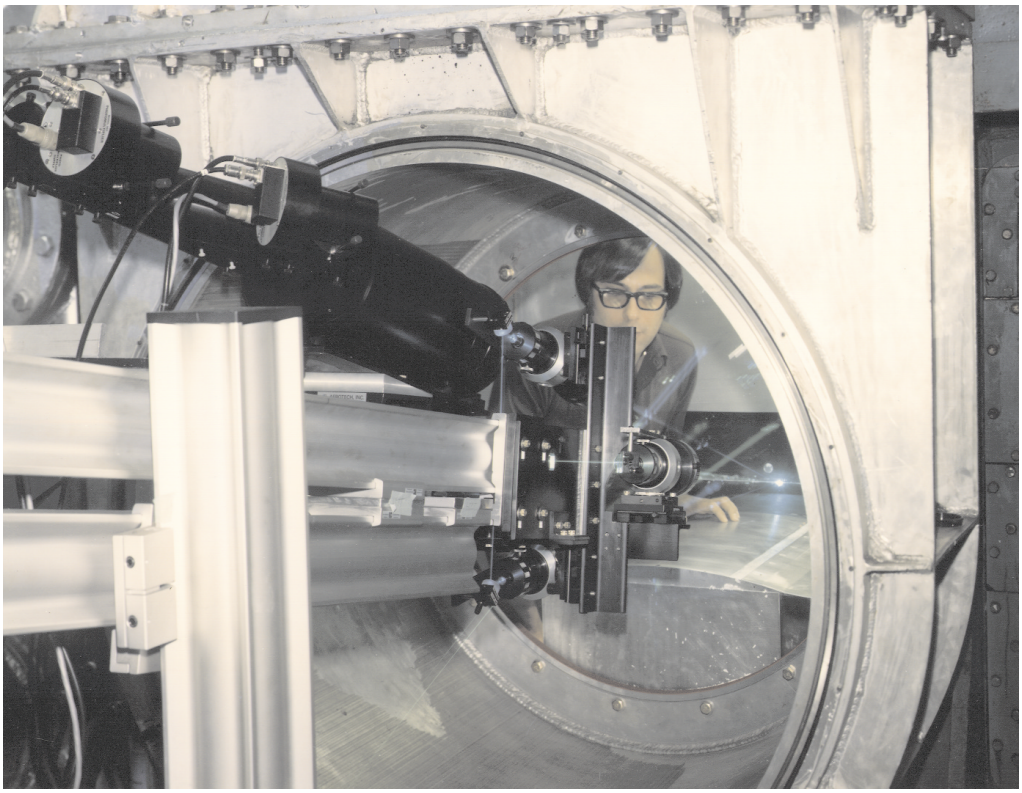

Figure 4.- Tunnel Installation of the Laser Velocimeter.

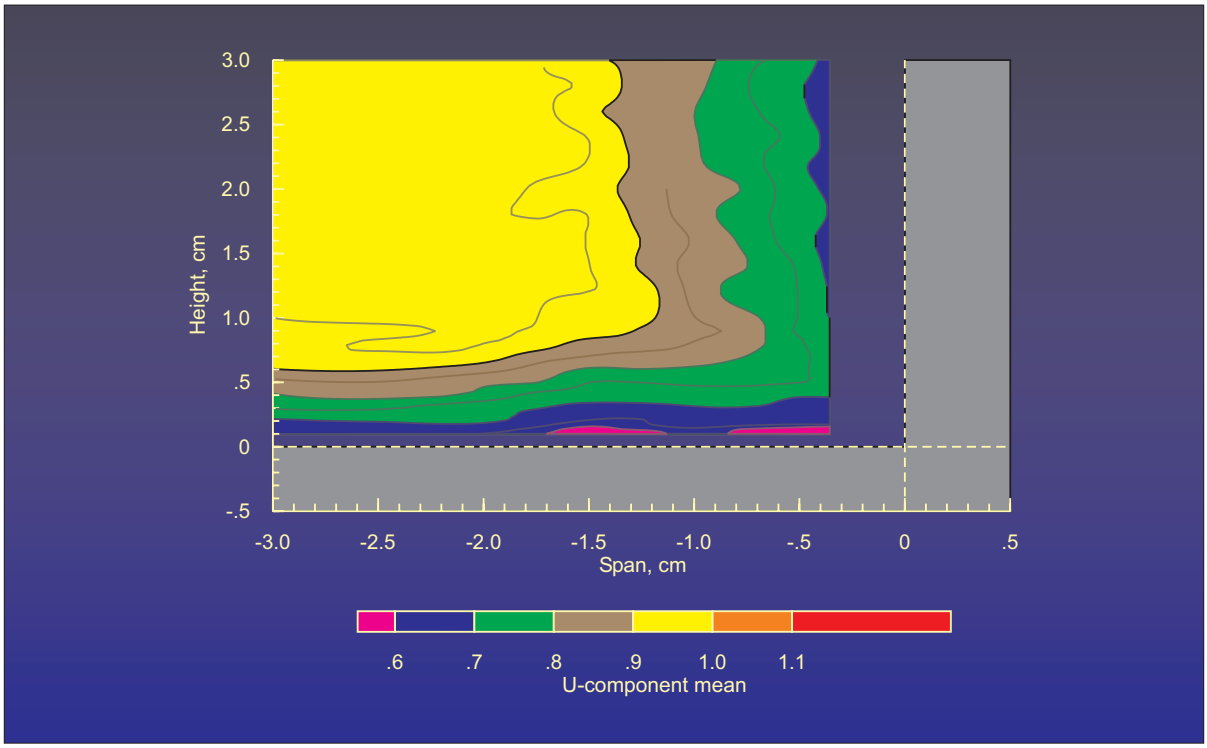


Figure 5.- Mean Velocity U-component (Max = 33.4 m/sec, Min = 17.4 m/sec).

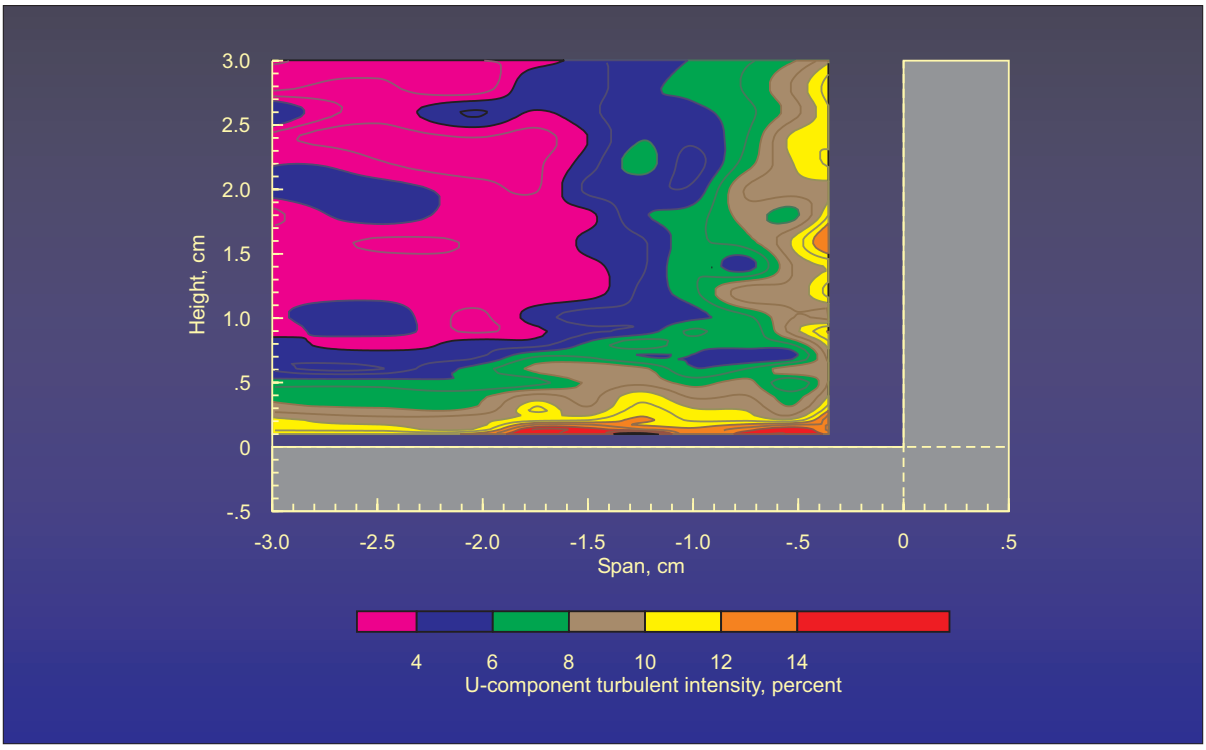


Figure 6.- Turbulence Intensity, U-component (Max = 0.174, Min = 0.029).

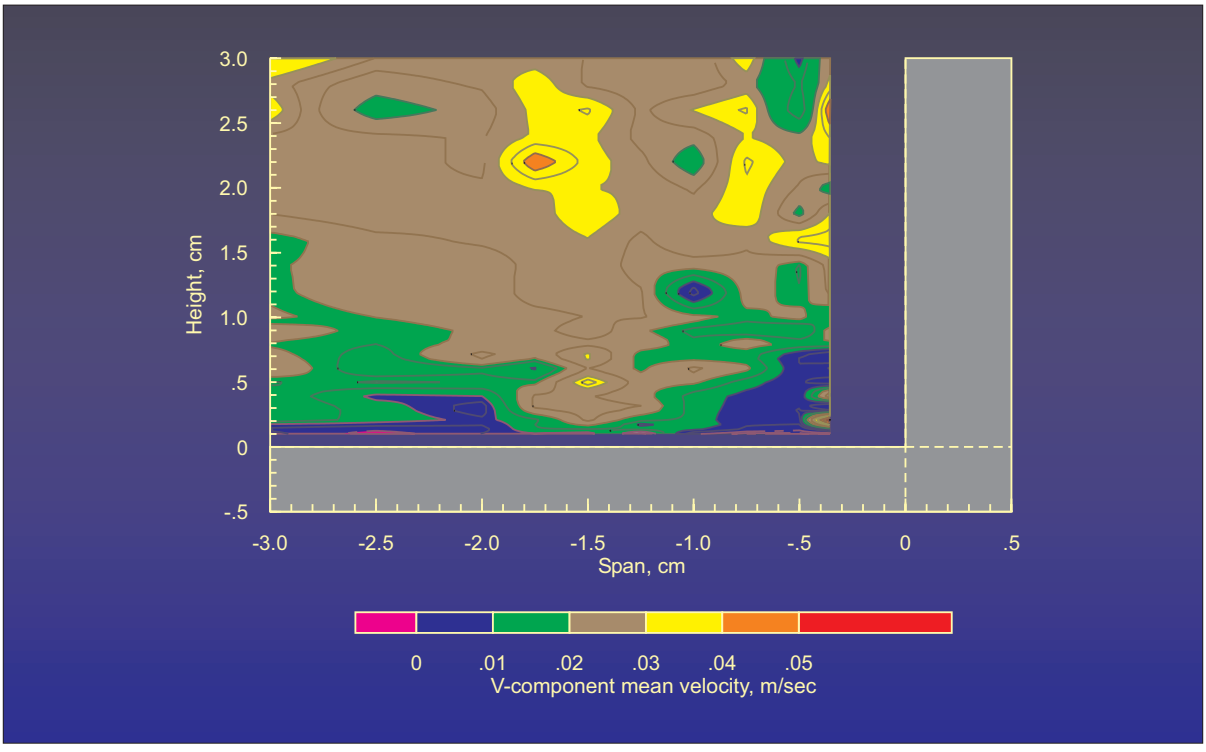


Figure 7.- Mean Velocity, V-component (Max = 1.1 m/sec, Min = -1.0 m/sec).

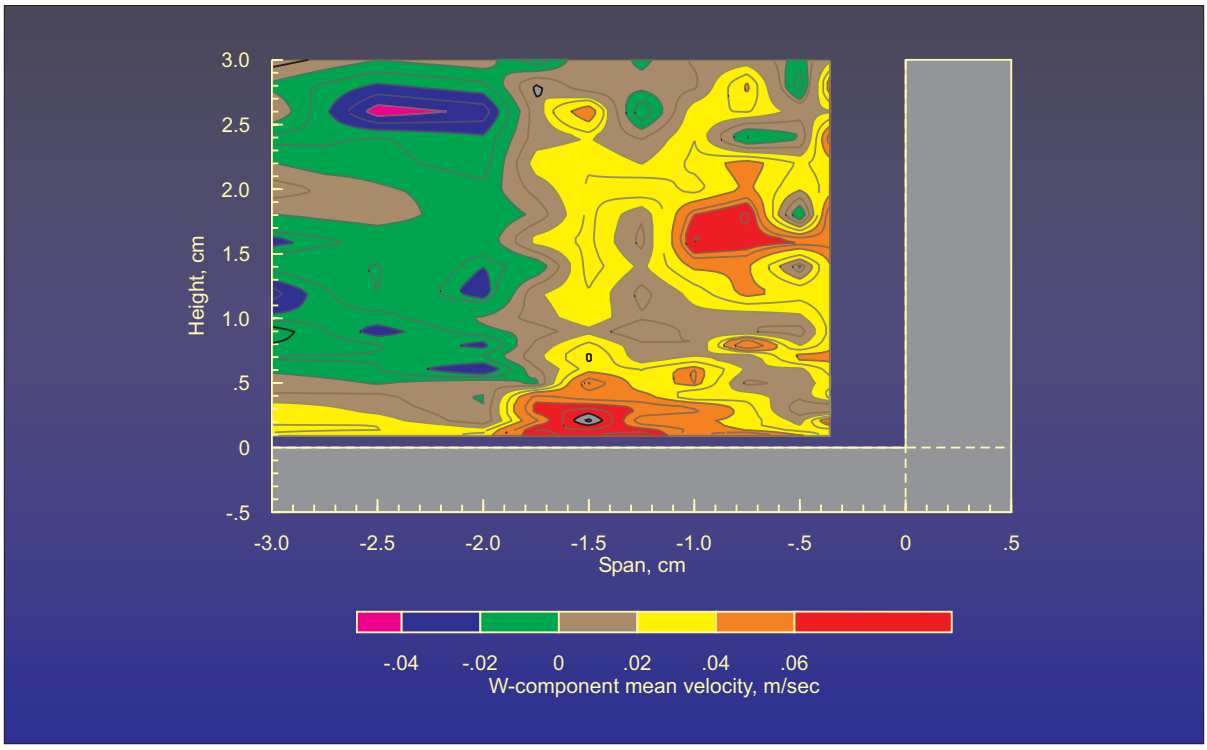


Figure 8.- Mean Velocity, W-component (Max = 2.4 m/sec, Min = -1.7 m/sec).

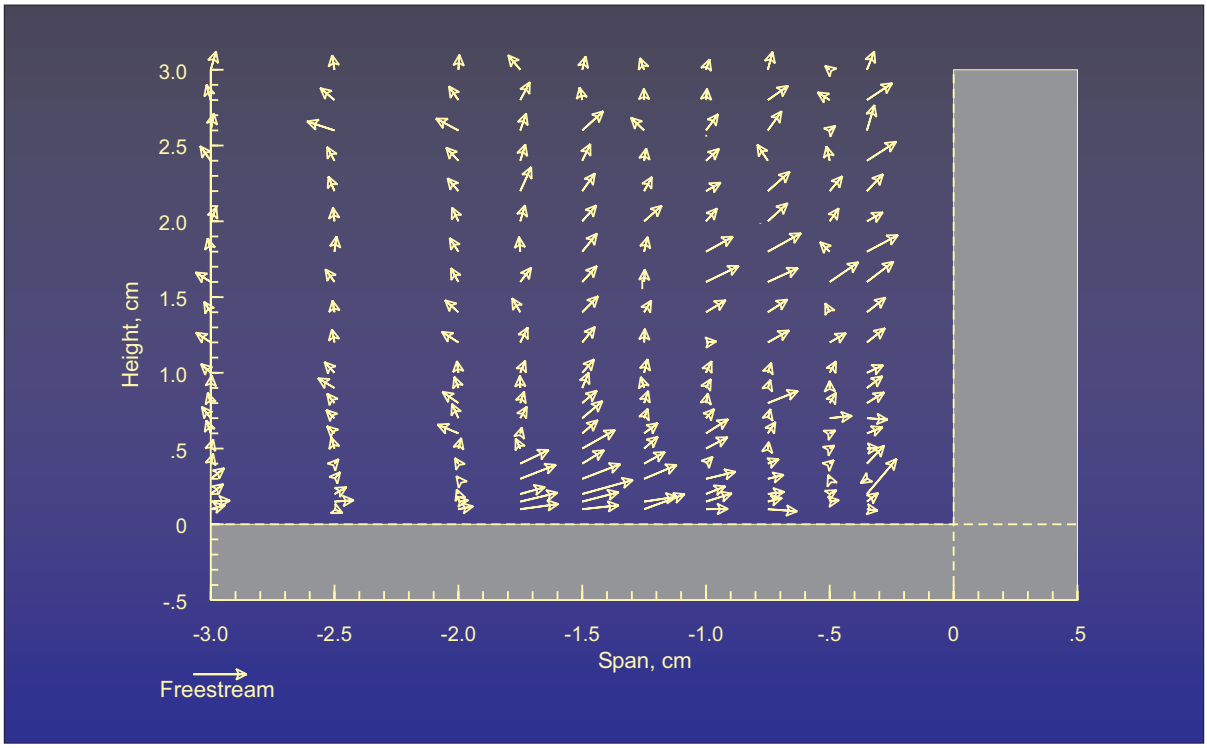


Figure 9.- Velocity Vector Plot.

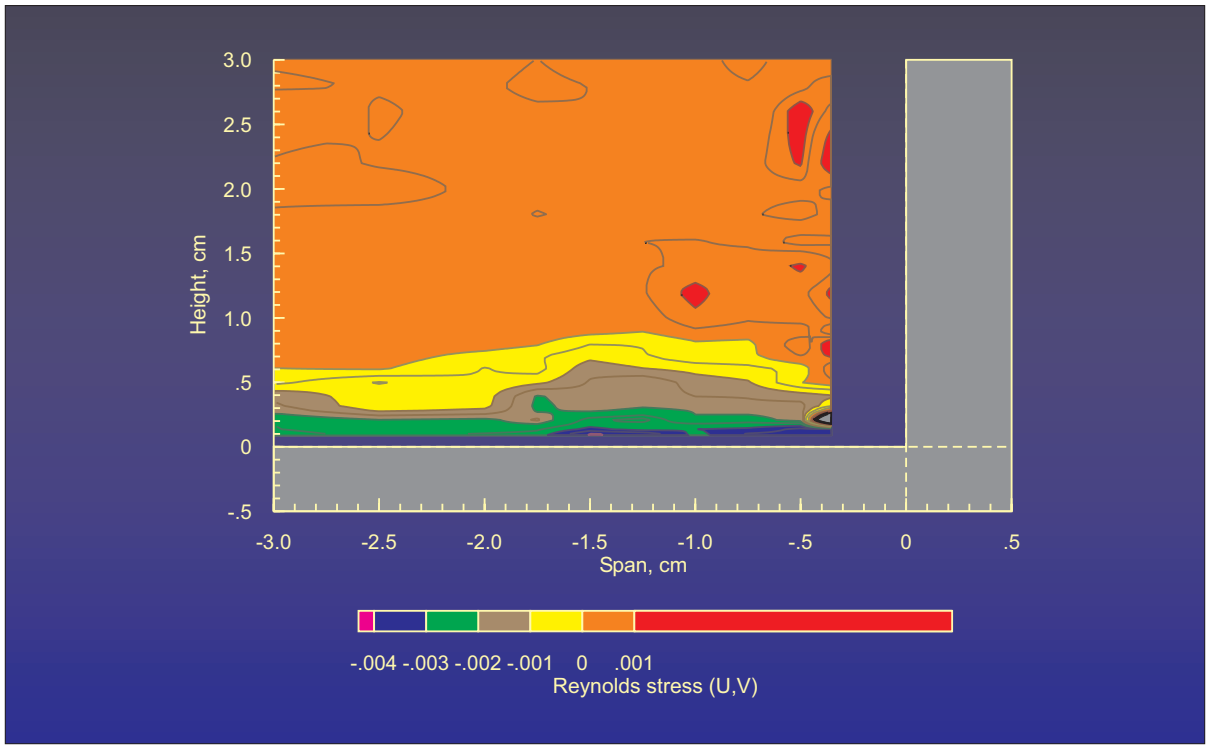


Figure 10.- Reynolds Stress (U,V) (Max = 0.001, Min = -0.001).

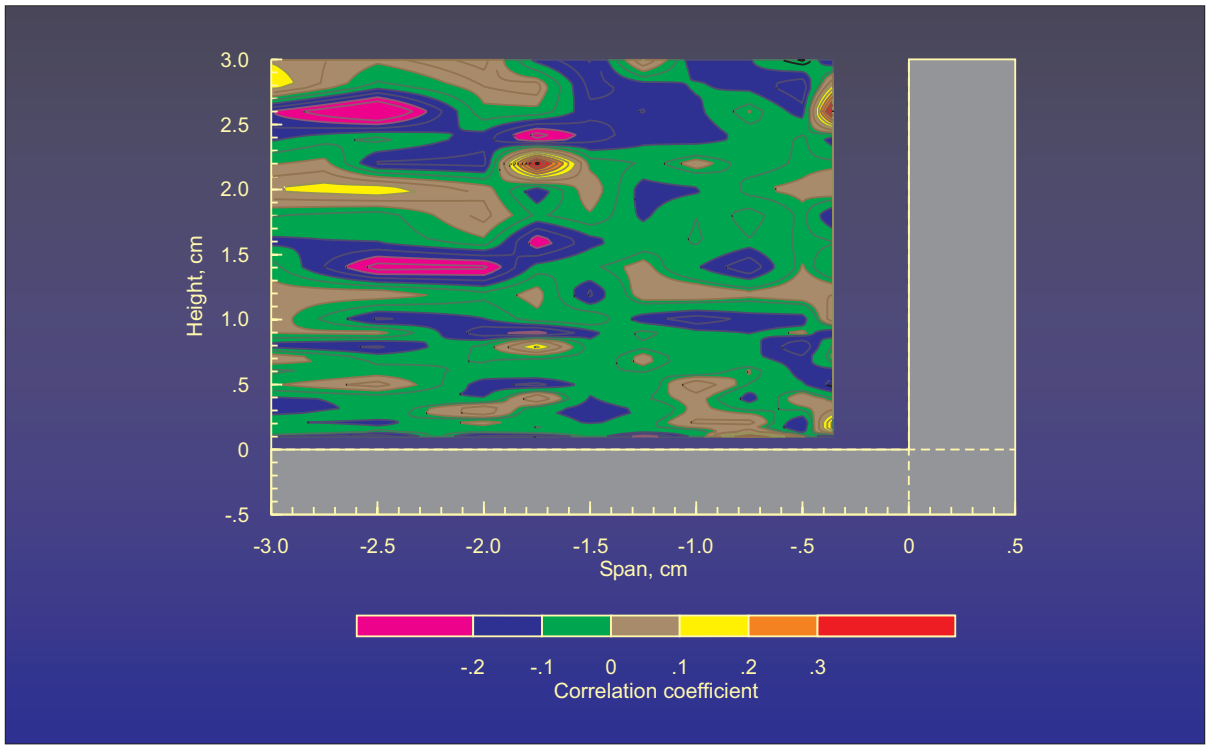


Figure 11.- Correlation Coefficient (U:data rate) (Max = 0.43, Min = -0.32).